

# Nonlinear domain wall resonance in garnet films with perpendicular anisotropy: Critical role of nonlinear damping

N. Vukadinovic\*

*Dassault Aviation, 78 quai Marcel Dassault, 92552 St-Cloud, France*

J. Ben Youssef and N. Beaulieu

*Université de Bretagne Occidentale, Laboratoire de Magnétisme de Bretagne CNRS, 29285 Brest, France*

V. Castel

*Telecom Bretagne, Technopole Iroise-Brest, CS83818, 29238 Brest, France*

(Received 27 February 2015; revised manuscript received 11 September 2015; published 7 December 2015)

Domain wall resonance spectra in the weakly nonlinear regime for garnet films with a perpendicular anisotropy supporting parallel stripe domains have been investigated using micromagnetic simulations and zero-field broadband ferromagnetic resonance experiments. The main characteristics of the 2D numerical micromagnetic approach we developed is to solve the Landau-Lifshitz equation by an iterative method in the frequency domain and to incorporate a nonlinear phenomenological damping term. It is shown that the nonlinear damping affects simultaneously the driving field dependencies of the resonance frequency and the resonance linewidth for the fundamental domain wall resonance of parallel stripe domains, and the critical field for the domain wall resonance foldover. The micromagnetic simulations allow us to reproduce quantitatively both the nonlinear redshift of the domain wall resonance frequency and the nonlinear line broadening experimentally observed for increasing values of the input microwave power.

DOI: [10.1103/PhysRevB.92.214408](https://doi.org/10.1103/PhysRevB.92.214408)

PACS number(s): 75.60.Ch, 75.78.Cd, 76.50.+g

## I. INTRODUCTION

Magnetic films with a perpendicular anisotropy are promising systems for various applications in high-density storage media [1], spintronics devices [2,3], or skyrmion-hosting materials without the Dzyaloshinskii-Moriya interaction [4]. One striking feature of such films is the existence of a regular stripe domain pattern at zero magnetic field according to the film thickness and its quality factor  $Q$  defined as  $Q = K_u/2\pi M_s^2$ , where  $K_u$  is the uniaxial perpendicular anisotropy constant and  $M_s$  the saturation magnetization [5]. Nowadays, a critical point both for fundamental physics and for applications is to get a deep understanding of the nonlinear high-frequency dynamics in such films with nonuniform magnetization configurations. This issue can be tackled by considering monocrystalline garnet films with a large quality factor  $Q > 1$  as a model system. In this case, it is possible to stabilize as a micromagnetic ground state a parallel stripe domain pattern consisting of nearly homogeneous up and down magnetized domains separated by narrow domain walls (DWs). The excitation spectrum in the linear regime of parallel stripe domains in garnet films with  $Q > 1$  has been extensively studied [6,7]. One powerful tool for measuring it is to excite the stripe domain pattern by means of a small-amplitude rf magnetic field and to detect the rf power absorption. It is well known that the absorption spectra exhibit multiple DW and domain resonances depending on the pumping field orientation [8–10].

On the other hand, the nonlinear dynamics of parallel stripe domains can be probed by increasing the amplitude of the driving field. Such measurements were conducted at the beginning of the 1980s. Regarding the DW resonances,

a downshift (redshift) of the resonance frequency for the fundamental DW resonance [11], the parametric excitation of DW waves [12,13], and the saturation of the resonance line amplitude [13] were experimentally evidenced using a magneto-optical detection. From the theoretical viewpoint, the nonlinear dynamics of DWs in a parallel stripe pattern has been investigated by considering either a nonlinear potential energy or a nonlinear kinetic energy. In the former case, the nonlinear response of DWs has been analyzed in detail by means of a one-dimensional equation of motion for the DW displacement including a nonlinear restoring force due to the magnetic charges at the film surfaces [14–16]. According to the amplitude of the rf exciting field, periodic, quasiperiodic, and chaotic DW oscillations have been predicted [15]. In the last case, the kinetic energy relies on a change of the internal DW structure. It was recognized that for a film with a large quality factor  $Q > 1$ , the kinetic nonlinearity is predominant with respect to the potential nonlinearity [11,17] and is responsible for the observed redshift. However, a quantitative comparison between experience and modeling regarding the nonlinear DW resonance spectra in terms of resonance frequency and resonance linewidth is still lacking. Moreover, Tiberkevich and Slavin [18] have proposed a new phenomenological damping term to represent the nonlinear dissipation torque in the Landau-Lifshitz equation. This formalism succeeded in explaining the nonlinear dissipation rate in current-driven in-plane magnetized ferromagnetic nanopillars [18], the existence condition for the foldover of the ferromagnetic resonance (FMR) line [19,20] in Permalloy strips, and, partially, the nonlinear FMR resonance linewidth in yttrium iron garnet films (YIG) [21]. An intriguing question is now to know to what extent this formalism can be applied for analyzing the nonlinear DW spectra.

\*nicolas.vukadinovic@dassault-aviation.com

In this context, this paper aims at investigating the fundamental DW resonance in a weakly nonlinear regime for garnet films with a perpendicular anisotropy supporting parallel stripe domains by means of micromagnetic simulations and broadband FMR measurements at zero magnetic field. Much attention is paid to the effect of the nonlinear damping on the main features of the rf power dependent DW resonance spectra (resonance frequency shift, resonance line broadening). It is shown from the comparisons between the experimental data and the simulations results that the nonlinear damping term plays a critical role in reproducing the experimental data.

The paper is organized as follows. Section II presents the micromagnetic model and the numerical method for solving the nonlinear Landau-Lifshitz equation for magnetization motion in the frequency domain. Two phenomenological representations for the magnetic dissipation have been considered: the standard linear Gilbert damping term and the nonlinear damping term proposed by Tiberkevich and Slavin [18]. The results of micromagnetic simulations conducted for the case of a thin garnet film exhibiting a stripe domain pattern are then reported. The computed evolutions of the frequency shift and the resonance linewidth for the fundamental DW resonance as the amplitude of the rf exciting field increases are displayed. The linear and nonlinear damping dependencies of the critical field for DW resonance foldover are presented as well. Section III is devoted to experimental results coming from the broadband FMR and the comparisons with the micromagnetic simulations for a garnet film with a stripe domain pattern. The limitations of the phenomenological approach of the nonlinear DW damping are discussed in Sec. IV. Conclusions are drawn in Sec. V.

## II. MICROMAGNETIC SIMULATIONS

### A. Model

Modeling of the rf magnetic field driven absorption spectrum in the nonlinear regime for magnetic films or elements with nonuniform magnetization configurations is a challenging problem. The most powerful and general approach is based on micromagnetic simulations. So far, the standard procedure consists of integrating the Landau-Lifshitz-Gilbert equation for magnetization motion in the time domain in the presence of a temporal exciting magnetic field to obtain the temporal response of the magnetization configuration [22–28]. The time-averaged absorbed power is usually computed by integrating over one or several periods of the driving field the dot product of the temporal excitation and the temporal magnetization [26]. In the present work, two innovative developments have been carried out. First, the nonlinear damping term suggested by Tiberkevich and Slavin [18] has been introduced in the micromagnetic simulations. Second, an alternate iterative method was developed for solving the nonlinear Landau-Lifshitz equation in the frequency domain. This one generalizes the method of successive approximations [29] used for spatially uniform magnetization states. On the other hand, this two-dimensional (2D) micromagnetic approach extends the one previously reported for computing the dynamic susceptibility spectra (linear regime) of films with nonuniform magnetization configuration [30,31]. The method saves the

same advantages. (i) The power absorption spectrum can be easily refined within spectral ranges including resonance lines. This results in high-accuracy determinations of the resonance frequency, resonance linewidth, and maximum amplitude for each line. (ii) The spatial map of the dynamic magnetization at the resonance frequency of each line (mode structure) is a direct output of simulations. (iii) The time for computing a spectrum around a resonance line is independent of the spectral position of the line. This method is briefly described hereafter.

Let us consider a static magnetization configuration  $\mathbf{M}_{eq}(\mathbf{r}) = M_s \mathbf{m}_{eq}(\mathbf{r})$ , where  $\mathbf{r}$  is the position vector and  $M_s$  the saturation magnetization. After applying a uniform exciting magnetic field  $\delta \mathbf{h}(t)$ , the time evolution of equilibrium state is described by the Landau-Lifshitz equation:

$$\frac{\partial \mathbf{m}(\mathbf{r}, t)}{\partial t} = -|\gamma| [\mathbf{m}(\mathbf{r}, t) \times \mathbf{H}_{eff}(\mathbf{r}, t)] + \mathbf{T}(\mathbf{r}, t), \quad (1)$$

where  $\mathbf{H}_{eff}(\mathbf{r}, t)$  is the total effective field including the contributions from the demagnetizing, Zeeman, exchange, and anisotropy fields, and  $\mathbf{T}(\mathbf{r}, t)$  is the damping torque. In what follows, the generalized nonlinear damping torque proposed by Tiberkevich and Slavin [18] is considered:

$$\mathbf{T}(\mathbf{r}, t) = \alpha(\zeta) \left[ \mathbf{m}(\mathbf{r}, t) \times \frac{\partial \mathbf{m}(\mathbf{r}, t)}{\partial t} \right], \quad (2)$$

where the standard Gilbert damping parameter  $\alpha$  is replaced by the damping function  $\alpha(\zeta)$  with  $\zeta$  defined as

$$\zeta = \frac{1}{\omega_M^2} \left( \frac{\partial \mathbf{m}(\mathbf{r}, t)}{\partial t} \right)^2, \quad (3)$$

and  $\omega_M = \gamma 4\pi M_s$ .

After a Taylor series expansion of  $\alpha(\zeta)$  and by restricting ourselves to the linear term in  $\zeta$ , the nonlinear damping torque takes the form

$$\mathbf{T}(\mathbf{r}, t) = \alpha \left[ 1 + \frac{q_1}{\omega_M^2} \left( \frac{\partial \mathbf{m}(\mathbf{r}, t)}{\partial t} \right)^2 \right] \left[ \mathbf{m}(\mathbf{r}, t) \times \frac{\partial \mathbf{m}(\mathbf{r}, t)}{\partial t} \right], \quad (4)$$

where  $q_1$  is the dimensionless expansion coefficient characterizing the first-order nonlinear correction in the damping function, satisfying the criterion  $q_1 \zeta \ll 1$ .

The dynamic magnetization and the effective field can be split as follows separating the static and dynamic terms:

$$\mathbf{m}(\mathbf{r}, t) = \mathbf{m}_{eq}(\mathbf{r}) + \delta \mathbf{m}(\mathbf{r}, t), \quad (5)$$

$$\mathbf{H}_{eff}(\mathbf{r}, t) = \mathbf{H}_{eq}(\mathbf{r}) + \mathbf{H}_{eff}(\delta \mathbf{m}) + \delta \mathbf{h}(t), \quad (6)$$

where  $\mathbf{H}_{eq}(\mathbf{r}) = \mathbf{H}_{eff}(\mathbf{m}_{eq})$  is the static effective field. Assuming harmonic time dependencies for  $\delta \mathbf{m}$  and  $\delta \mathbf{h}$ , Eq. (1) can be expanded as follows using Eqs. (5) and (6) and remembering the equilibrium condition  $\mathbf{m}_{eq} \times \mathbf{H}_{eq} = 0$ :

$$\begin{aligned} & -\frac{i\omega}{|\gamma|} \delta \mathbf{m} + \left( \mathbf{H}_{eq} + \frac{i\alpha\omega}{|\gamma|} \mathbf{m}_{eq} \right) \times \delta \mathbf{m} \\ & - \mathbf{m}_{eq} \times \mathbf{H}_{eff}(\delta \mathbf{m}) - \mathbf{m}_{eq} \times \delta \mathbf{h} \\ & + (\mathbf{H}_{eff}(\delta \mathbf{m}) + \delta \mathbf{h}) \times \delta \mathbf{m} \\ & + \frac{i\alpha\omega}{|\gamma|} q_1 \left( \frac{\omega}{\omega_M} \right)^2 |\delta \mathbf{m}|^2 (\mathbf{m}_{eq} \times \delta \mathbf{m}) = 0, \quad (7) \end{aligned}$$

where the first two lines correspond to the first-order term in  $\delta\mathbf{m}$  and  $\delta\mathbf{h}$ , and the last two to higher-order terms.

Introducing the linear operator  $L$ ,

$$L\delta\mathbf{m} = \left( -\frac{i\omega}{|\gamma|}I + D_2 - D_1 D_H \right) \delta\mathbf{m}, \quad (8)$$

where  $I$  is the unit operator and the operators  $D_1$ ,  $D_2$ , and  $D_H$  are defined, for any given vector  $\mathbf{v}$ , by [30]

$$\begin{aligned} D_1\mathbf{v} &= \mathbf{m}_{eq} \times \mathbf{v}, \\ D_2\mathbf{v} &= \left( \mathbf{H}_{eq} + \frac{i\alpha\omega}{|\gamma|}\mathbf{m}_{eq} \right) \times \mathbf{v}, \\ D_H\mathbf{v} &= \mathbf{H}_{eff}(\mathbf{v}), \end{aligned} \quad (9)$$

and the nonlinear operator  $N$ ,

$$\begin{aligned} N(\delta\mathbf{m}) &= (\mathbf{H}_{eff}(\delta\mathbf{m}) + \delta\mathbf{h}) \times \delta\mathbf{m} \\ &+ \frac{i\alpha\omega}{|\gamma|}q_1 \left( \frac{\omega}{\omega_M} \right)^2 |\delta\mathbf{m}|^2 (\mathbf{m}_{eq} \times \delta\mathbf{m}), \end{aligned} \quad (10)$$

the left-hand side of Eq. (7) takes the form

$$F(\delta\mathbf{m}) = L\delta\mathbf{m} + N(\delta\mathbf{m}) - D_1\delta\mathbf{h}, \quad (11)$$

and the Landau-Lifshitz equation with the nonlinear damping term can be recast in the nonlinear equation

$$F(\delta\mathbf{m}) = 0. \quad (12)$$

Various strategies can be foreseen to solve Eq. (12). For our 2D problems, the solution  $\delta\mathbf{m}$  is found using the discrete Newton method [32]. Using a regular spatial grid with  $n$  discretization points,  $\mathbf{m}$ ,  $\mathbf{m}_{eq}$ ,  $\delta\mathbf{m}$ ,  $\mathbf{H}_{eq}$ ,  $\mathbf{H}_{eff}$ , and  $\delta\mathbf{h}$  are  $3n$  vectors and  $F$  becomes a complex vector-valued function  $\mathbf{F}$ . Writing  $\delta\mathbf{m} = \{\delta m_1, \dots, \delta m_{3n}\}$ , and  $\mathbf{F} = \{F_1, \dots, F_{3n}\}$ , the  $k$ th Newtonian iteration is defined by

$$B(\delta\mathbf{m}^k)\mathbf{s}^{(k)} = -\mathbf{F}(\delta\mathbf{m}^k), \quad (13)$$

where the matrix  $B$  is a finite difference approximation of the Jacobian matrix  $J$ :

$$J_{ij} = \frac{\partial F_i(\delta\mathbf{m})}{\partial \delta m_j}, \quad i, j = 1, \dots, 3n, \quad (14)$$

and

$$\mathbf{s}^{(k)} = \delta\mathbf{m}^{(k+1)} - \delta\mathbf{m}^{(k)}. \quad (15)$$

Solving the linear system Eq. (13) leads to the update solution  $\delta\mathbf{m}^{(k+1)}$ . A sequence of terms  $\delta\mathbf{m}^{(k)}$   $k = 1, \dots, p$  is generated and the convergence is reached when the reduced modulus satisfies

$$\frac{|\mathbf{s}^{(p)}|}{|\delta\mathbf{m}^{(p)}|} < \epsilon, \quad (16)$$

where  $\epsilon$  is a given error. The initial solution  $\{\delta\mathbf{m}^{(0)}\}$  is obtained by solving the linear equation

$$L\delta\mathbf{m}^0 = D_1\delta\mathbf{h}. \quad (17)$$

This procedure is applied for each angular frequency  $\omega$ . The microwave absorption power  $P_a$  is then computed by the general expression

$$P_a = \frac{1}{2} \text{Re} \left[ i\omega \int_V dV \delta\mathbf{h} \cdot \delta\mathbf{m}^* \right], \quad (18)$$

where the asterisk denotes the complex conjugation and  $V$  the sample volume. For our 2D problems, the sum is restricted to the cross-sectional surface  $S$ .

From the practical standpoint, several points merit being highlighted. (i) Assembling the dense matrix  $B$  represents the predominant computational cost with respect to solving the linear system Eq. (13). Consequently, the discrete Newton method is appropriate for 2D micromagnetic simulations where the number of unknowns is typically lower than  $10^4$ . For larger systems as those usually encountered for 3D micromagnetic simulations, alternate iterative methods with preconditioning but without forming and storing the Jacobian matrix have to be preferred [33]. (ii) The main advantages are the robustness of the method and its speed of convergence. In our case, no more than 40 iterations were necessary to reach convergence for all the conducted simulations with  $\epsilon = 10^{-4}$  and within the explored range of  $|\delta\mathbf{h}|$  values.

## B. Numerical results

The micromagnetic simulations were conducted by considering a magnetic garnet film with a perpendicular anisotropy. The material parameters are the following: the exchange constant  $A = 2 \times 10^{-7}$  erg/cm, the saturation induction  $4\pi M_S = 500$  G, the uniaxial perpendicular anisotropy constant  $K_u = 14\,000$  erg/cm<sup>3</sup> ( $Q \sim 1.4$ ), the gyromagnetic ratio  $\gamma = 1.8 \times 10^7$  s<sup>-1</sup> Oe<sup>-1</sup>, the Gilbert damping parameter  $\alpha = 0.02$ , and the film thickness  $t = 0.25$   $\mu\text{m}$ . The small cubic anisotropy existing in garnet films is neglected in the micromagnetic simulations. The zero-field micromagnetic ground state for such a film is a parallel stripe domain pattern with a stripe period  $P_0$  as depicted in Fig. 1(a). For 2D micromagnetic simulations, the  $z$  axis corresponds to the elongation direction of the stripe domains (invariant axis), the  $x$  axis to the in-plane direction normal to the stripe domains, and the  $y$  axis to the film normal. The computations were performed using periodic boundary conditions along the  $x$  axis. So, the system is reduced to the periodic cell of size  $P_0 \times t$ . The used mesh sizes along the  $x$  and  $y$  axis are  $\Delta_x = 7.7$  nm and  $\Delta_y = 15.6$  nm, respectively. These values are lower than the smallest length scale for magnetic films with  $Q > 1$ , namely, the Bloch DW width parameter  $\Delta_0 = (A/K_u)^{1/2} = 37.8$  nm. The computed equilibrium magnetization configuration over one period of the stripe pattern is reported in Fig. 1(b). It consists of up (magnetized along the  $+y$  axis) and down (magnetized along the  $-y$  axis) domains (see the  $m_y$  component) separated by a 2D DW with a Bloch character at the film center (see the  $m_z$  component) and a Néel character at the film surfaces (see the  $m_x$  component). The equilibrium stripe period  $P_0$  and the associated spatial magnetization configuration correspond to the lowest 2D micromagnetic energy. The optimized  $P_0$  value is equal to 1.35  $\mu\text{m}$ .

In this work, we focus on the fundamental DW resonance (Bloch type) excited by a rf magnetic field applied along the film normal [30]. The micromagnetic simulations in the nonlinear regime were carried out using first the linear Gilbert damping parameter and then the nonlinear one as defined in Eq. (4). Hereafter, the results will be presented using two quantities: the local dynamic magnetization component  $\delta m_y(x, y)$  and the spatial average of this term,

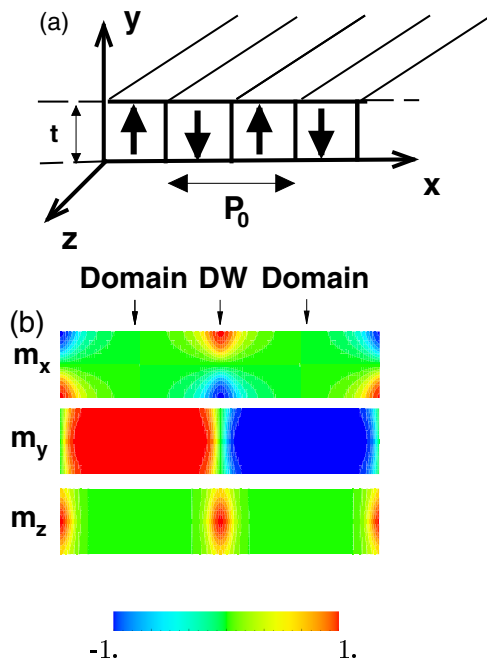


FIG. 1. (Color online) (a) Schematic representation of the parallel stripe domain pattern for a film of thickness  $t$  with a perpendicular magnetic anisotropy and coordinate system.  $P_0$  is the zero-field spatial period of stripe domains. (b) Cross-sectional views of the static magnetization components  $m_x$ ,  $m_y$ , and  $m_z$  over one period of the stripe domain pattern computed by 2D micromagnetic simulations for the film under consideration ( $Q \simeq 1.4$ ).

$$\langle \delta m_y \rangle = \frac{1}{S} \int_S \delta \mathbf{m} \cdot \mathbf{u}_y dS, \text{ where } \mathbf{u}_y \text{ is the unit vector along the } y \text{ axis and } S = P_0 \times t.$$

### 1. Nonlinear DW resonance with linear damping

Figure 2(a) displays the frequency dependence of the imaginary part of the average dynamic magnetization component  $\langle \delta m_y \rangle$ , termed  $\text{Im}(\langle \delta m_y \rangle)$  for increasing values of the rf driving field amplitude  $\delta h_y$  ranging from 5 mOe up to 35 mOe. For  $\delta h_y = 5$  mOe (linear regime), the spectrum reveals a unique resonance line within the frequency band 150 MHz to 190 MHz, located at the frequency  $f_r = 172.6$  MHz. The map of  $\text{Im}(\delta m_y)$  in the  $(x, y)$  plane computed at the resonance frequency allows us to assign this line to the Bloch DW mode [see Fig. 2(b)]. As the pumping field amplitude increases, the symmetric resonance line transforms progressively into an asymmetric one. The resonance frequency is shifted towards the low frequencies (redshift). For  $\delta h_y = 35$  mOe, the resonance frequency reaches the value  $f_r = 169.3$  MHz resulting in a lowering of 2.5%. The mode structure remains unchanged as shown in Fig. 2(b). The essential difference is the downward shift of the phase of  $\langle \delta m_y \rangle$ . Figure 2(c) shows that this phase is equal to  $90^\circ$  for  $\delta h_y = 1$  mOe (linear regime) in agreement with the standard damped harmonic oscillator model for DW oscillations [6] and decreases quadratically down to  $64.5^\circ$  for  $\delta h_y = 35.3$  mOe. The variation of the resonance frequency with  $\delta h_y$  is plotted in Fig. 2(d). The downshift is nicely fitted by a quadratic law. A vertical slope for the  $\text{Im}(\langle \delta m_y \rangle)$  curve is achieved for  $\delta h_y = 36$  mOe, which corresponds to the critical

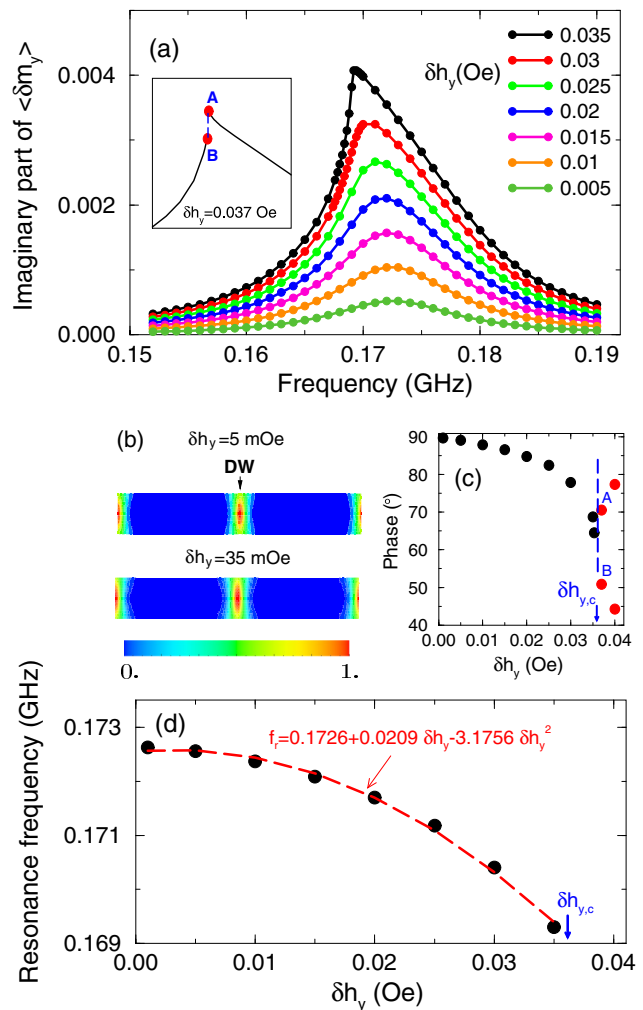


FIG. 2. (Color online) Fundamental nonlinear DW resonance computed by micromagnetic simulations with linear damping. (a) Imaginary part of the average dynamic magnetization component  $\langle \delta m_y \rangle$  as a function of the pumping field frequency for various values of the pumping field amplitude  $\delta h_y$ . (b) Spatial distribution of the imaginary part of the dynamic magnetization component  $\delta m_y(x, y)$  over one period of the stripe domain pattern computed at each resonance frequency for  $\delta h_y = 5$  mOe (linear regime) and  $\delta h_y = 35$  mOe (nonlinear regime). For each case, the imaginary part of  $\delta m_y(x, y)$  is normalized by its maximum value. (c) Phase of  $\langle \delta m_y \rangle$  as a function of  $\delta h_y$ . The critical field for the DW resonance foldover  $\delta h_{y,c}$  is indicated by the arrow. The points A and B refer to the inset in panel (a). (d) DW resonance frequency versus  $\delta h_y$ . The dashed line is the best quadratic fit.

rf field for the DW resonance foldover,  $\delta h_{y,c}$ . Above this value, a jump appears in the  $\text{Im}(\langle \delta m_y \rangle)$  curve that becomes bivalued. As an illustration, the inset in Fig. 2(a) evidences such a jump between the points A and B for the spectrum computed at  $\delta h_y = 37$  mOe. These two solutions for the DW dynamics are distinguished by the amplitudes of  $\text{Im}(\langle \delta m_y \rangle)$  [see the inset in Fig. 2(a)] and the phases of  $\langle \delta m_y \rangle$  [see Fig. 2(c)]. For larger  $\delta h_y$  values, it is worth noting that the slopes of the phase versus  $\delta h_y$  have opposite signs for the two solutions. The evolution of the critical field for the DW resonance foldover as a function of

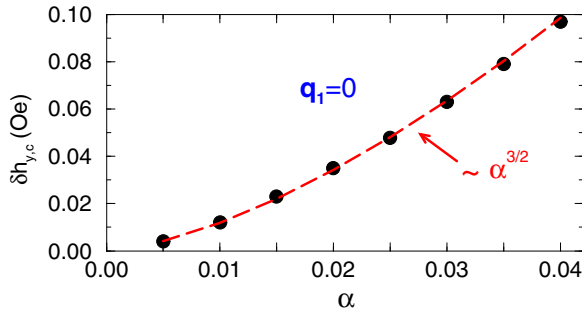


FIG. 3. (Color online) Evolution of the critical field for the DW resonance foldover  $\delta h_{y,c}$  with the Gilbert damping parameter  $\alpha$ . The dashed line is the best power-law fit.

the damping parameter  $\alpha$  is displayed in Fig. 3. This variation scales as  $\alpha^{3/2}$ .

At this stage, it is instructive to compare these results with those known for the perpendicular FMR (perpendicularly magnetized thin films) in the nonlinear regime. The standard model, based on the cone angle approximation for the uniform precession mode [34], predicts a quadratic decrease of the resonance field, or equivalently a quadratic increase (blueshift) of the resonance frequency for increasing the driving field amplitude [19,20]. The sense of the shift is opposite to that observed for the DW resonance. However, the direction and the amplitude of the FMR shift may be changed due to the magnetocrystalline anisotropy [35] or more generally to the effective field [36]. Recently, the correlation between the downshift of the resonance field for FMR and the phase of the uniform mode for increasing values of the rf driving field has been experimentally pointed out by time-resolved FMR measurements for thin Permalloy films [37]. Such a correlation is clearly confirmed by our micromagnetic simulations for the nonlinear DW resonance. Lastly, the critical field for the FMR foldover varies like  $\alpha^{3/2}$  as well [19,20,34]. However, it should be noted that the inadequacy of that model for describing quantitatively the FMR foldover has been extensively discussed [38] and introduction of a nonlinear damping has been proposed leading to very good agreement between theory and experience [19,20]. The effect of a nonlinear damping on the DW resonance in the nonlinear regime is numerically addressed in the next section.

## 2. Nonlinear DW resonance with nonlinear damping

The frequency dependence of  $\text{Im}(\langle \delta m_y \rangle)$  for various values of  $\delta h_y$ , computed with the nonlinear damping term defined in Eq. (4) with  $q_1 = 100$ , is reported in Fig. 4(a). It is worth noting that for the case under consideration, the condition  $q_1(\omega/\omega_M)^2|\delta \mathbf{m}|^2 < 1$  is fulfilled for the investigated frequency and rf field amplitude ranges. Asymmetric resonance profiles and the redshift of the resonance frequency are again clearly observed. However, introduction of the nonlinear damping term leads to new features, namely, (i) a weaker variation of the resonance frequency and a less asymmetric resonance line for a given value of  $\delta h_y$ , (ii) an upward shift of the critical field for the DW resonance foldover ( $\delta h_{y,c} = 90.5$  mOe for  $q_1 = 100$ ), and (iii) as expected, a significant broadening of the DW resonance line. The mode structure remains similar to

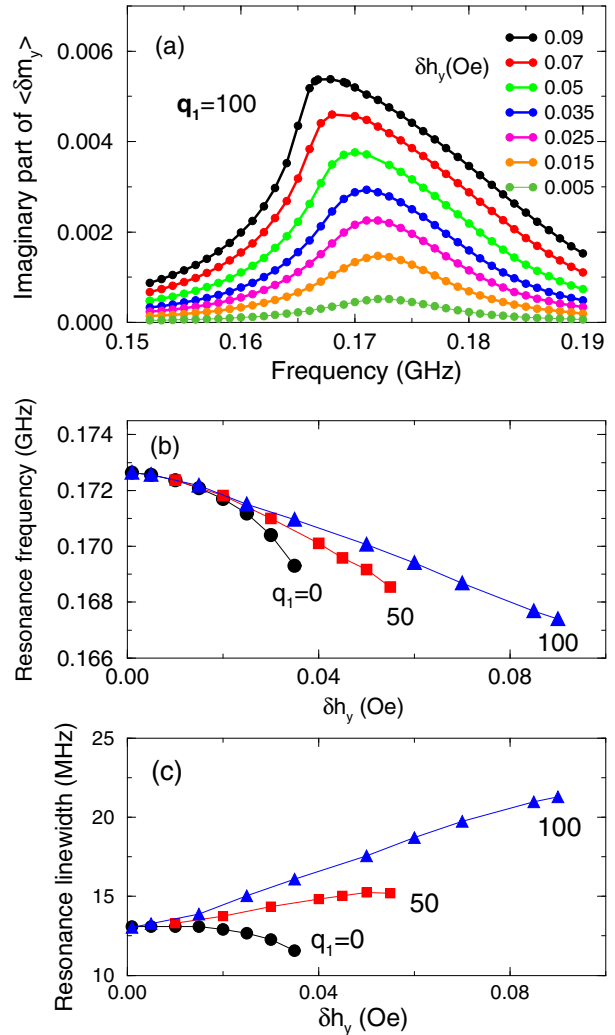


FIG. 4. (Color online) Fundamental nonlinear DW resonance computed by micromagnetic simulations with nonlinear damping. (a) Imaginary part of the average dynamic magnetization component  $\langle \delta m_y \rangle$  as a function of the pumping field frequency for various values of the pumping field amplitude  $\delta h_y$ . The nonlinear damping parameter is fixed at  $q_1 = 100$ . (b) DW resonance frequency versus  $\delta h_y$  for various  $q_1$  values. (c) DW resonance linewidth versus  $\delta h_y$  for various  $q_1$  values. The solid lines are guides to the eyes.

those shown in Fig. 2(b) and the phase of  $\langle \delta m_y \rangle$  decreases more slowly with respect to the case  $q_1 = 0$ , from  $89.1^\circ$  for  $\delta h_y = 5$  mOe down to  $76.3^\circ$  for  $\delta h_y = 90$  mOe. More precisely, the evolution of the resonance frequency as a function of  $\delta h_y$  is displayed in Fig. 4(b) for  $q_1 = 0$  (linear damping),  $q_1 = 50$ , and  $q_1 = 100$ . As  $q_1$  increases, the quadratic law for the resonance frequency downshift is changed and tends progressively to a quasilinear law for the largest  $\delta h_y$  values. The variation of the resonance linewidth (full width at half maximum) with  $\delta h_y$  for  $q_1 = 0$ ,  $q_1 = 50$ , and  $q_1 = 100$  is shown in Fig. 4(c). For the linear damping, the resonance linewidth is independent of  $\delta h_y$ , except in the vicinity of the critical field for the DW resonance foldover. In this case, the resonance line is strongly distorted and appears to be shrunk [see Fig. 2(a)]. As  $q_1$  increases, the driving field amplitude dependence of the resonance linewidth is getting more and

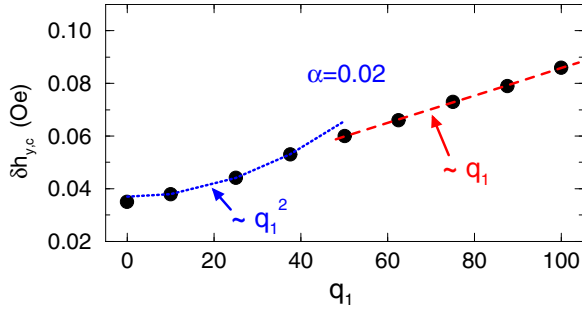


FIG. 5. (Color online) Evolution of the critical field for the DW resonance foldover  $\delta h_{y,c}$  with the nonlinear damping parameter  $q_1$ . The dotted line corresponds to the quadratic fit ( $q_1 < 50$ ) whereas the dashed line is the linear fit ( $q_1 \geq 50$ ).

more strong. The resonance linewidth follows a quasilinear variation with  $\delta h_y$  for the largest  $\delta h_y$  values. For  $q_1 = 100$ , the linewidth is raised up by a factor 1.7 with respect to the linear case. Figure 5 displays the evolution of the critical field for the DW resonance foldover as a function of  $q_1$ . The Gilbert damping parameter is fixed at  $\alpha = 0.02$ . It is shown that  $\delta h_{y,c}$  increases with  $q_1$ . Two regimes can be distinguished: a quadratic variation for  $q_1 \leq 35$  and a quasilinear slope for  $q_1 > 35$ .  $\delta h_{y,c}$  is increased by a factor 2.4 between the two extreme  $q_1$  values ( $q_1 = 0$  and  $q_1 = 100$ ). From these numerical results, it can be concluded that both the slopes of the resonance frequency and the resonance linewidth versus  $\delta h_y$  reflect the degree of nonlinearity for the dissipative term. In addition, the critical field for the DW resonance foldover is strongly correlated with the nonlinear damping parameter.

Let us come back to the nonlinear FMR. The improved model including a cone angle dependence for the FMR linewidth [19,20] is based on the generalized damping term proposed by Tiberkevich and Slavin [18]. In this case, the FMR linewidth in the nonlinear regime reads as  $\Delta H_{NL} = \beta 4\pi M_s \theta^2$ , where  $\beta$  is a dimensionless parameter which depends on frequency, and  $\theta$  is the cone angle for the uniform precession. The critical field for the FMR foldover  $\delta h_c$  is expressed by [19,20]:  $\delta h_c^2 = [(1 + 4\beta^2)/(1 - 2\sqrt{3}\beta)]^3$  within the parameter range  $\beta < 1/(2\sqrt{3})$  where the foldover effect exists. This gives rise to a strong increase of  $\delta h_c$  when  $\beta$  approaches the limit value  $\beta = 1/(2\sqrt{3})$ . This behavior departs from the smoother variation of  $\delta h_{y,c}$  with  $q_1$  observed for the nonlinear DW resonance.

### III. EXPERIMENTAL RESULTS

#### A. Materials

The investigated sample is a single-crystal garnet film with a perpendicular anisotropy grown by liquid phase epitaxy on a (111)-oriented gadolinium gallium garnet (GGG) substrate.

The film composition and material parameters are gathered in Table I. The saturation magnetization  $M_s$  was determined with a vibrating sample magnetometer (VSM). Ferromagnetic resonance (FMR) measurements (linear regime) in the perpendicular configuration (polarizing field along the film normal) were used to identify the uniaxial perpendicular anisotropy constant  $K_u$  and the gyromagnetic ratio  $\gamma$  from the linear variation of the resonance frequency with field, and the damping constant  $\alpha$  from the linear frequency dependence of the FMR resonance linewidth. The exchange constant  $A$  at room temperature  $T_R$  was inferred from the theoretical law [39]:  $A = A_{YIG}(T_N - T_R)/(T_{N,YIG} - T_R)$ , where  $T_N$  and  $T_{N,YIG}$  are the Néel temperatures for our substituted YIG film and for a pure YIG film, respectively, and  $A_{YIG}$  is the exchange constant of pure YIG at room temperature. For  $T_{N,YIG} = 560$  K,  $T_N = 425$  K (estimate for our composition), and  $A_{YIG} = 4.15 \times 10^{-7}$  erg/cm, this leads to  $A = 2 \times 10^{-7}$  erg/cm. The weak contribution of the cubic magnetocrystalline anisotropy ( $|K_1|/K_u \sim 0.05$ , where  $K_1$  is the first-order cubic anisotropy constant) will be neglected hereafter. The parallel stripe domain pattern was nucleated using a demagnetizing process under both perpendicular and parallel magnetic fields [40]. The measured zero-field stripe domain period  $P_0$  is reported in Table I as well. For the comparison between experiment and simulation, the computations were conducted using the magnetic parameters reported in Table I except for the damping parameter. Indeed, it was shown [10] that the value of the Gilbert damping parameter  $\alpha = 0.008$ , greater than that deduced from the FMR measurements ( $\alpha = 0.002$ ), is needed to fit the experimental the DW resonance linewidth in the linear regime. The value  $\alpha = 0.008$  was hence adopted for the micromagnetic simulations.

#### B. DW resonance spectra

The DW resonance measurements were performed within the frequency range [20 MHz to 1 GHz] using a highly sensitive broadband spectrometer with a nonresonant 50  $\Omega$  microstrip reflection line. This 1-mm-wide microstrip line is fed by a microwave current that generates the rf exciting field. The selected pumping field configuration corresponds to a predominant in-plane component of the rf exciting field parallel to the stripe domain direction. An out-of-plane component of the rf exciting field along the film normal exists at the microstrip lateral edges [see Fig. 6(a)]. The input microwave power  $P$  was varied from  $10^{-2}$  mW up to 150 mW. To enhance the sensitivity of the DW resonance signal, a frequency modulation and a lock-in amplifier were employed resulting in the derivative power absorption spectra  $dP_a/df$ .

The experimental rf power dependence of the derivative absorption spectra is displayed in Fig. 6(b). Within the

TABLE I. Set of material parameters for the used garnet sample.

Composition	$M_s$ (emu/cm <sup>3</sup> )	$K_u$ (erg/cm <sup>3</sup> )	$\gamma$ (s <sup>-1</sup> Oe <sup>-1</sup> )	$\alpha$	$t$ ( $\mu$ m)	$P_0$ ( $\mu$ m)
Y <sub>1.8</sub> Bi <sub>0.63</sub> Lu <sub>0.56</sub> Fe <sub>4.18</sub> Al <sub>0.83</sub> O <sub>12</sub>	43.8	$1.84 \times 10^4$	$1.78 \times 10^7$	$2 \times 10^{-3}$	0.5	1.5

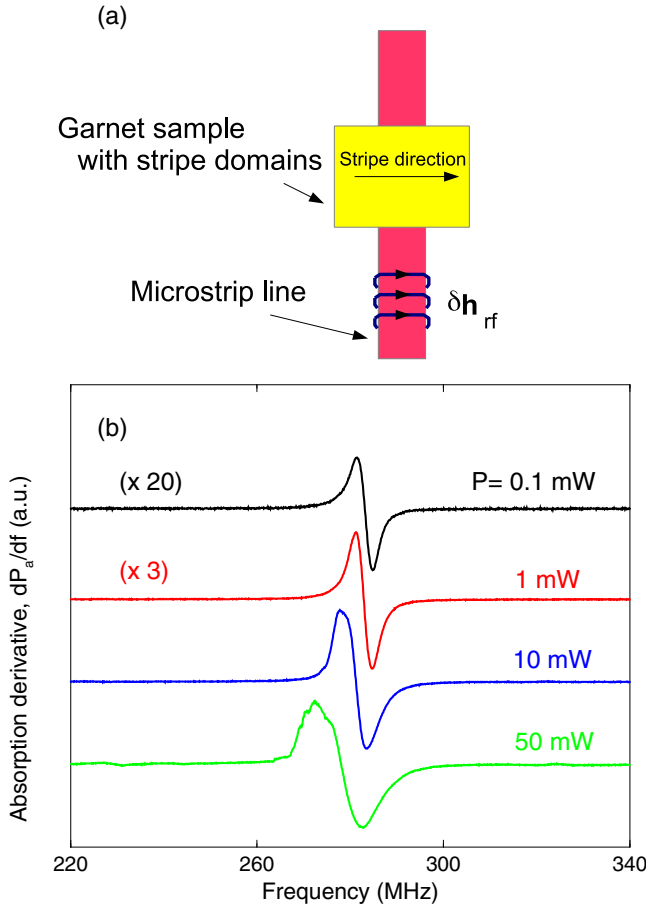


FIG. 6. (Color online) DW resonance measurements in linear and nonlinear regimes. (a) Sketch of the setup for DW resonance measurements. The garnet sample with a parallel stripe domain pattern is situated above the rf microstrip line. The predominant component of the in-plane rf exciting field is parallel to the direction of stripe domains. (b) Derivative microwave absorption spectra for various input rf power levels  $P$ . The amplification factors are labeled in the parentheses.

frequency range 220–340 MHz, the low-level power spectrum ( $P = 10^{-1}$  mW) consists of a unique well-defined resonance line at frequency  $f_r = 283$  MHz, previously identified as the fundamental Bloch DW (BDW) resonance mode [10]. This line cannot be excited by the in-plane component of the rf exciting field but only by the small out-of-plane component for this pumping field configuration. For increasing  $P$  values, the resonance frequency of the BDW mode is shifted towards the low frequencies and the resonance line is broadened [Fig. 6(b)]. These spectra are characterized by a weak asymmetry of the resonance line and the absence of foldover. Furthermore, small oscillations are clearly observed on the positive part of the resonance line for the spectrum recorded at  $P = 50$  mW. Upon increasing the spectral resolution (reduced modulation amplitude), this fine structure was previously identified as standing elastic modes in the film/substrate system [41]. Two additional results merit being highlighted. (i) The amplitude of the BDW resonance line saturates at around  $P = 100$  mW. This effect has been previously interpreted as the consequence of horizontal Bloch line nucleation within the DW [13]. (ii) The

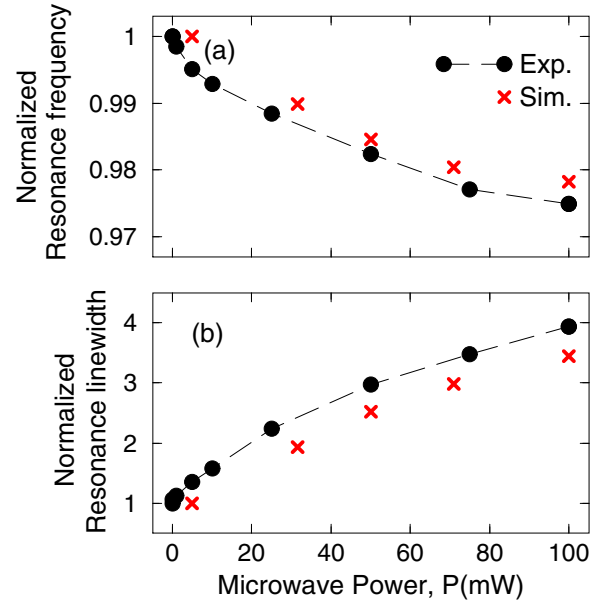


FIG. 7. (Color online) Comparisons between experimental data and results of micromagnetic simulations. (a) Reduced DW resonance frequency as a function of the input microwave power  $P$ . The resonance frequencies are normalized by that in the linear regime ( $P = 10^{-2}$  mW). (b) Reduced peak-to-peak DW resonance linewidth as a function of  $P$ . The resonance linewidths are normalized by that in the linear regime. The symbols are related to measurements. The dashed lines are guides to the eyes. The results of micromagnetic simulations are displayed by cross symbols.

DW resonance spectra is independent of the frequency sweep direction for the explored values of the input rf power. These results are consistent with those obtained by a magneto-optical detection technique [11].

The evolutions of the resonance frequency and resonance linewidth as a function of  $P$  are reported in Figs. 7(a) and 7(b), respectively. The resonance frequency (resp. resonance linewidth) at a given power  $P$  is normalized by that measured in the linear regime ( $P = 10^{-2}$  mW). A nonlinear decrease of the resonance frequency and a nonlinear increase of the resonance linewidth are observed for increasing  $P$ . These behaviors depart from those that would be expected assuming a linear damping term, namely, a linear dependence of the resonance frequency with  $P$  and no dependence of the resonance linewidth as function of  $P$  for the investigated power range (see Fig. 4). This justifies the requirement of a nonlinear damping term.

Let us now turn on the quantitative comparison between the experimental data and the results of micromagnetic simulations. First of all, it is necessary to estimate the correspondence between the incident microwave power  $P$  and the rf magnetic field, in particular the normal component  $\delta h_y$  exciting the DW resonance. The input power is proportional to  $\delta h_y^2$ , or equivalently,  $\delta h_y^2 = kP$ , where  $k$  is the coupling parameter depending on the geometrical features of the microstrip line. For our setup, a reasonable value for  $k$  is  $633 \text{ A}^2/(\text{W m}^2)$  (which corresponds to  $\delta h_y = 10$  mOe for  $P = 1$  mW). Figure 7(a) shows the comparison between the experimental and numerical evolutions of the normalized resonance

frequency as a function of the microwave power. The micromagnetic simulations enable us to reproduce the experimental nonlinear decrease using the nonlinear damping parameter  $q_1 = 200$ . Figure 7(b) displays the variation of the experimental and numerical normalized peak-to-peak linewidth with  $P$ . Once again, the results of micromagnetic simulations are in very good agreement with the experimental data using the same  $q_1$  value. It should be mentioned that both for the resonance frequency and for the resonance linewidth, the microwave power dependencies are reproduced in terms of profiles and amplitudes.

#### IV. DISCUSSION

The results presented in Fig. 7 show that the nonlinear term suggested in Ref. [18] allows us to account for the rf power dependencies of the DW resonance frequency and the DW resonance linewidth. However, it should be remarked that the selected value  $q_1 = 200$  is rather large compared to that previously reported for the nonlinear current-driven precession in ferromagnetic layers [18] ( $q_1 = 3$ ) and results in a nonlinear correction  $q_1 \zeta \simeq 1$ . This means that the nonlinear dissipative part is of the same order of magnitude as its linear counterpart. Recently, the nonlinear FMR in YIG films was analyzed using the same nonlinear damping term and a value  $q_1 = 250$  was found to match partially the experimental resonance linewidth [21] which corresponds, once again, to an equivalent weight between the linear and nonlinear dissipative terms. For the nonlinear FMR, the validity of this used phenomenological nonlinear damping term and its link with microscopic relaxation mechanisms were previously discussed [18,20]. It was shown that this nonlinear model can be applied even in magnetic systems where the nonlinear magnon-magnon relaxation processes are dominant [18]. For our case of DW resonances in a parallel stripe domain structure, multiple channels of relaxation exist. Besides the direct relaxation to thermal magnons or phonons, largely studied for the case of isolated DWs [42,43], indirect relaxation mechanisms through interaction of DW waves are operative. Based on a DW-wave model [44], the dispersion surfaces  $f_{r,n}(k_{\parallel}, k_{\text{perp}})$  for the fundamental DW mode ( $n = 0$ ) and higher-order flexural DW modes ( $n > 0$ ) were calculated in the linear regime [13], where  $f_{r,n}$  is the resonance frequency for the considered DW mode, and  $k_{\parallel}$  and  $k_{\text{perp}}$  are the components of the DW wave vector parallel and perpendicular to the in-plane direction of stripe domains, respectively. From these dispersion surfaces, it was shown that DW waves with  $k_{\parallel} \neq 0$  and  $k_{\text{perp}} \neq 0$  exist at half frequency of the fundamental DW wave mode ( $k = 0$ ) making possible a parametric excitation of DW waves through a three-DW-wave interaction mechanism. This splitting process is equivalent to the first-order Suhl instability for the FMR [45]. Such parametric DW excitations were experimentally evidenced by a magneto-optical technique [12,13]. Parametric DW wave resonances excited through nonlinear coupling are also pointed out in our experimental DW resonance spectra above a critical input rf power  $P_c \sim 25$  mW as shown in Fig. 8. In addition to the fundamental DW excitation at the resonance frequency  $f_r$ , a small-amplitude signal is revealed at  $f_r/2$ . Other nonlinear DW wave interactions can be foreseen from the dispersion

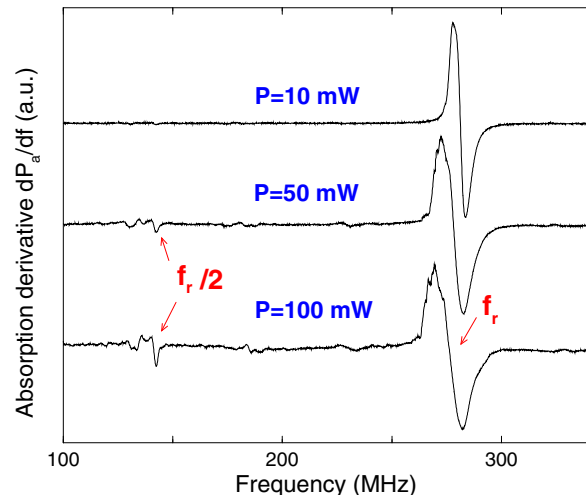


FIG. 8. (Color online) Derivative absorption spectrum within a wider frequency range for various input rf power showing the fundamental nonlinear DW resonance at the frequency  $f_r$  and the subsidiary nonlinear DW resonance at  $f_r/2$  (parametric excitation of DW waves) appearing above  $P = 25$  mW.

surfaces: a two-DW-wave interaction [46] (equivalent to the two-magnon scattering in FMR [47]) and a four-DW-wave interaction [13] (similar to the four-magnon scattering process evidenced in YIG microstructures [48] and thin metallic films [49]). Our 2D micromagnetic simulations cannot account rigorously for such mechanisms changing the number of DW-wave magnons with  $k \neq 0$  and involving oblique DW wave vectors. The required high values of  $q_1$  to match the experimental data could reflect artificially such nonlinear DW relaxation mechanisms. To support this assumption, it has been established that the dominant nonlinear four-magnon scattering process in thin ferromagnetic films can be described using an effective Gilbert-type damping term [49].

To go further, two issues would deserve to be more deeply investigated in the near future. First, the existence of a spatially nonuniform magnetic texture entails an enhancement of the dyadic dissipation as demonstrated by Thiele [50]. In addition, the dynamical change of this texture due to the DW motion in the nonlinear regime has a feedback on this dyadic dissipation as well. These effects are taken into account by the micromagnetic simulations based on a purely phenomenological generalized Gilbert model assuming local and isotropic dissipation mechanisms described by the scalar  $\alpha$  and  $q_1$  parameters. However, recent investigations of magnetic damping in conducting ferromagnets with a noncollinear magnetization pointed out an anisotropic texture-enhanced Gilbert damping [51,52] both in linear and nonlinear regimes [53]. It would be interesting to study the relevance of using linear and nonlinear anisotropic damping terms for our insulating garnet films.

Second, an important open question is to know whether the findings obtained by our frequency domain approach with a nonlinear damping differ (and to what extent) from those that would result from a direct integration in the time domain of the nonlinear Landau-Lifshitz-Gilbert equation with a linear damping term using a high-power field excitation. In the last

case, a nonlinear contribution to the magnetic dissipation arises from the nonlinear dynamic magnetization and its time derivative. Unfortunately, such time domain micromagnetic simulations of nonlinear DW spectra with a high enough spectral resolution lead to costly computation time due partly to the low-lying DW excitation and were not conducted in the present work. However, it should be remarked that, as shown in Ref. [18], using the standard Gilbert damping constant in the nonlinear regime can result in inconsistent nonlinear behaviors. Indeed, the magnetic dissipation is proportional to frequency in the framework of the Gilbert model. For magnetic systems with a nonlinear redshift of the resonance frequency, this results in a decrease of the time rate of the energy loss for increasing the excitation amplitude in opposition to most of the microscopic relaxation processes. Taking into account a nonlinear damping allows removing this inconsistency.

## V. SUMMARY AND CONCLUDING REMARKS

By means of micromagnetic simulations and zero-field broadband FMR measurements, the DW resonance spectra in the weakly nonlinear regime have been investigated for garnet films with a perpendicular anisotropy supporting a parallel stripe domain pattern. The nonlinear DW response in such systems reveals two intimately correlated behaviors, namely, the redshift of the fundamental DW resonance frequency and the

broadening of this resonance line as the input rf field or power increases. The 2D micromagnetic simulations conducted in the frequency domain and including a generalized Gilbert-type dissipation term (first-order nonlinear dissipation model) allow us to reproduce quantitatively the nonlinear power dependencies of the redshift and the line broadening experimentally observed. In addition, the micromagnetic simulations show that the nonlinear damping term controls both the amplitudes and profiles of these two quantities as a function of the rf driving solicitation and, consequently, the critical field for the DW resonance foldover. These results have been established for the model system of parallel stripe domain pattern in low-loss garnet films. It should be interesting to investigate the nonlinear high-frequency response of metallic magnetic films or micro/nanostructures with a perpendicular anisotropy (for instance, FePt, CoPt, FePd binary alloys) envisaged for high-density storage media and spintronics devices to test the robustness of the phenomenological nonlinear damping term used in the present work. From the theoretical point of view, it would be interesting to investigate the effect of the second-order nonlinear dissipation term on the nonlinear DW dynamics in stripe domain structures.

## ACKNOWLEDGMENTS

N.V. thanks M. Labrune for the static micromagnetic simulations.

- 
- [1] J. H. Franken, H. J. M. Swagten, and B. Koopmans, *Nat. Nanotechnol.* **7**, 499 (2012).
  - [2] S. Ideka, K. Mura, H. Yamamoto, K. Mizunuma, H. Gan, M. Endo, S. Kanai, J. Hayakawa, and H. Ohno, *Nat. Mater.* **9**, 721 (2010).
  - [3] R. Sbiaa, H. Meng, and S. N. Piramanayagam, *Phys. Status Solidi* **5**, 413 (2011).
  - [4] N. Nagaosa and Y. Tokura, *Nat. Nanotechnol.* **8**, 899 (2013).
  - [5] A. Hubert and R. Schaeffer, *Magnetic Domains* (Springer, Berlin, 1998).
  - [6] A. P. Malozemoff and J. C. Slonczewski, *Magnetic Domain Walls in Bubble Materials* (Academic Press, New York, 1979).
  - [7] U. Ebels, L. D. Buda, K. Ounadjela, and P. E. Wigen, *Spin Dynamics in Confined Magnetic Structures I* (Springer, Berlin, 2002).
  - [8] M. Ramesh and P. E. Wigen, *J. Magn. Magn. Mater.* **74**, 123 (1988).
  - [9] N. Vukadinovic, J. Ben Youssef, and M. Labrune, *Phys. Rev. B* **66**, 132418 (2002).
  - [10] N. Vukadinovic, J. Ben Youssef, V. Castel, and M. Labrune, *Phys. Rev. B* **79**, 184405 (2009).
  - [11] W. Jantz, B. E. Argyle, and J. C. Slonczewski, *IEEE Trans. Magn.* **16**, 657 (1980).
  - [12] J. H. Spreen and B. E. Argyle, *Appl. Phys. Lett.* **38**, 930 (1981).
  - [13] B. E. Argyle, J. C. Slonczewski, W. Jantz, J. H. Spreen, and R. H. Kryder, *IEEE Trans. Magn.* **18**, 1325 (1982).
  - [14] B. N. Filippov and M. M. Solov'ev, *Phys. Met. Metallogr.* **80**, 119 (1995).
  - [15] B. N. Filippov and M. M. Solov'ev, *Phys. Met. Metallogr.* **81**, 491 (1996).
  - [16] M. M. Solov'ev, B. N. Filippov, and A. N. Kalashnikov, *Phys. Met. Metallogr.* **81**, 495 (1996).
  - [17] A. K. Zvezdin, N. E. Kulagin, and V. G. Red'ko, *Phys. Met. Metallogr.* **45**, 37 (1979).
  - [18] V. Tiberkevich and A. Slavin, *Phys. Rev. B* **75**, 014440 (2007).
  - [19] Y. S. Gui, A. Wirthmann, N. Mecking, and C.-M. Hu, *Phys. Rev. B* **80**, 060402(R) (2009).
  - [20] Y. S. Gui, A. Wirthmann, and C.-M. Hu, *Phys. Rev. B* **80**, 184422 (2009).
  - [21] A. Y. Vidil, I. V. Zavislyak, and M. O. Popovh, *Ukr. J. Phys.* **59**, 141 (2014).
  - [22] G. Mohler, A. W. Hartner, and R. L. Moore, *J. Appl. Phys.* **93**, 7456 (2003).
  - [23] K.-S. Lee and S.-K. Kim, *Appl. Phys. Lett.* **91**, 132511 (2007).
  - [24] K. S. Buchanan, M. Grimsditch, F. Y. Fradin, S. D. Bader, and V. Novosad, *Phys. Rev. Lett.* **99**, 267201 (2007).
  - [25] M. Yan, P. Vavassori, G. Leaf, F. Y. Fradin, and M. Grimsditch, *J. Magn. Magn. Mater.* **320**, 1909 (2008).
  - [26] Y. Khivintsev, B. Kuanr, T. J. Fal, M. Haftel, R. E. Camley, Z. Celinski, and D. L. Mills, *Phys. Rev. B* **81**, 054436 (2010).
  - [27] A. Drews, B. Krüger, G. Selke, T. Kamionka, A. Vogel, M. Martens, U. Merkt, D. Möller, and G. Meier, *Phys. Rev. B* **85**, 144417 (2012).
  - [28] L. O'Brien, E. R. Lewis, A. Fernandez-Pacheco, D. Petit, R. P. Cowburn, J. Sampaio, and D. E. Read, *Phys. Rev. Lett.* **108**, 187202 (2012).
  - [29] A. G. Gurevich and G. A. Melkov, *Magnetization Oscillations and Waves* (CRC Press, Boca Raton, FL, 1996).
  - [30] N. Vukadinovic, O. Vacus, M. Labrune, O. Acher, and D. Pain, *Phys. Rev. Lett.* **85**, 2817 (2000).

- [31] N. Vukadinovic, M. Labrune, J. Ben Youssef, A. Marty, J. C. Toussaint, and H. Le Gall, *Phys. Rev. B* **65**, 054403 (2001).
- [32] J. M. Martinez, *J. Comput. Appl. Math.* **124**, 97 (2000).
- [33] S. A. Knoll and D. E. Keyes, *J. Comput. Phys.* **193**, 357 (2004).
- [34] P. W. Anderson and H. Suhl, *Phys. Rev.* **100**, 1788 (1955).
- [35] P. Gottlieb, *J. Appl. Phys.* **31**, 1059 (1969).
- [36] K. Gnatzig, H. Dotsch, M. Ye, and A. Brockmeyer, *J. Appl. Phys.* **62**, 4839 (1987).
- [37] H. G. Bauer, P. Majchrak, T. Rachel, C. H. Back, and G. Woltersdorf, [arXiv:1410.6993](https://arxiv.org/abs/1410.6993).
- [38] Y. K. Fetisov, C. E. Patton, and V. T. Synogach, *IEEE Trans. Magn.* **35**, 4511 (1999).
- [39] J. C. Slonczewski, A. P. Malozemoff, and E. A. Giess, *Appl. Phys. Lett.* **24**, 396 (1974).
- [40] H. Le Gall, N. Vukadinovic, J. Ostorero, and J. M. Desvignes, *J. Magn. Magn. Mater.* **84**, 229 (1990).
- [41] H. Dotsch and P. E. Wigen, *Solid State Commun.* **30**, 611 (1979).
- [42] J. F. Janak, *Phys. Rev.* **134**, A411 (1964).
- [43] A. S. Abyzov and B. A. Ivanov, *Sov. Phys. JETP* **49**, 865 (1979).
- [44] J. C. Slonczewski, *J. Magn. Magn. Mater.* **23**, 305 (1981).
- [45] H. Suhl, *J. Phys. Chem. Solids* **1**, 209 (1957).
- [46] N. Vukadinovic, A. Serraj, H. Le Gall, and J. Ben Youssef, *Phys. Rev. B* **58**, 385 (1998).
- [47] M. J. Hurben and C. E. Patton, *J. Appl. Phys.* **83**, 4344 (1998).
- [48] V. V. Naletov, G. de Loubens, V. Charbois, O. Klein, V. S. Tiberkevich, and A. N. Slavin, *Phys. Rev. B* **75**, 140405(R) (2007).
- [49] A. Y. Dobin and R. H. Victora, *Phys. Rev. Lett.* **90**, 167203 (2003).
- [50] A. A. Thiele, *Phys. Rev. Lett.* **30**, 230 (1973).
- [51] T. Weindler, H. G. Bauer, R. Islinger, B. Boehm, J. Y. Chauleau, and C. H. Back, *Phys. Rev. Lett.* **113**, 237204 (2014).
- [52] Z. Yuan, K. M. D. Hals, Y. Liu, A. A. Starikov, A. Brataas, and P. J. Kelly, *Phys. Rev. Lett.* **113**, 266603 (2014).
- [53] J. V. Kim, *Phys. Rev. B* **92**, 014418 (2015).